Materials for Renewable and Sustainable Energy (2019) 8:22
https://doi.org/10.1007/s40243-019-0160-1

ORIGINAL PAPER

Heteropolyacid ($H_3PW_{12}O_{40}$)-impregnated mesoporous KIT-6 catalyst for green synthesis of bio-diesel using transesterification of non-edible neem oil

P. Sudhakar[1] · **A. Pandurangan**[1]

Received: 6 July 2018 / Accepted: 6 November 2019 / Published online: 14 November 2019

Abstract
Mesoporous Ia3d cubic structured KIT-6 support was prepared by hydrothermal strategy and heteropoly acid content (10, 20 and 30%) was stacked on KIT-6 by wet-impregnation technique. The synthesized catalysts were characterized by XRD, N_2-sorption, NH_3-TPD, ATFT-IR, TEM and SEM–EDAX analyses. Acid properties of the supported catalysts were investigated by pyridine-adsorbed ATFT-IR and NH_3-TPD, respectively. Poly-anion coordination present in the catalyst was confirmed by the DRS-UV spectrum. The dispersion of heteropoly acid on the catalyst surface was observed by TEM analysis. Also, the presence of the elements such as W and P on the catalyst and its morphology were represented by the HRSEM–EDAX technique. The catalytic activity of HPWA/KIT-6 was investigated by the transesterification of neem oil with methanol. Among the different wt% catalyst, 20% catalyst showed highest neem oil conversion and selectivity at an optimized reaction temperature of 60 °C. Further, the spent catalyst was recovered and recycled three times, and it showed activity losses of less than 4%.

Keywords Mesoporous KIT-6 · Heteropolyacid · Non edible neem oil · Transesterification · Biodiesel

Introduction

The expansive usage of diesel fuels from petroleum derivative has made a serious ecological issue, which is environmental change and global warming [1]. Besides, the consuming of diesel fuel could discharge the toxin gasses, which are more destructive to the human well-being [2]. Further, energy security is considered as a fundamental factor in the decline of petroleum resources. Because of these environmental difficulties, sustainable and clean energy sources are pulled in enthusiasm for the worldwide [2]. The current study demonstrates that the usage of biofuel from sustainable resources can essentially lessen the emission of ozone harming substances, like greenhouse gases (GHG) by utilizing as a mix part of transportation fuel [3, 4]. Moreover, the significance of using biodiesel is its feasibility to reduce dependence on diesel. The mono-alkyl esters of long-chain fatty acids are called biodiesel, which is obtained from edible oil, non-edible oil and animal fats by the trans-esterification process [5]. Among the sustainable sources, non-edible oil sources are financially ideal in biodiesel generation, and it does not compete with the existing edible resources [6].

In this consideration, neem oil was an inexpensive feedstock for biodiesel production that effectively reduces production cost. Neem oil appears light to dark brown in color, has the strong pungent odor, and contains triglycerides with a huge quantity of triterpenoids, which was accountable for the bitter flavor. Also, it contains some steroids like campesterol, beta-sitosterol, and stigmasterol [7]. The composition of neem oil fatty acids was Palmitic (12.01 wt%), Stearic (12.95 wt%), Oleic (34.09 wt%), Linoleic (38.26 wt%) and Lignoceric (0.3 wt%) and their acid value was 44 mg KOH/g of oil [8]. Moreover, it was widely available in India and its subcontinent. The inedible neem oil was a promising alternative for edible oil. Further, the neem oil obtained from the neem tree was simply grown in any climate, and its seed contains 40% oil, which was more potential for biodiesel production [9]. Besides, the high content of monosaturated fatty acid in neem oil has shown good biodiesel characteristics

✉ A. Pandurangan
pandurangan_a@yahoo.com

[1] Department of Chemistry, Anna University, Chennai 600 025, India

[10]. However, the possible use of this oil in India is about 1 million tons per year [7].

Biodiesel synthesized by transesterification of vegetable oils and animal fats utilizing homogeneous acid and base catalyst has seen a fold augment in the most recent couple of years for their trade and use as a mixing part in transportation fuels. Indeed, the usage of homogeneous acid and base catalysts has created serious impediments in the reaction via corrosion and soap formation [11, 12]. Therefore, commercial biodiesel production utilizing ecologically well-disposed technique using heterogeneous catalysts has a significant interest in the industry. The production of biodiesel from non-edible oil via transesterification has been examined over numerous heterogeneous catalysts including metal oxides, sulphated zirconia, tungstated zirconia, etc. [13, 14]. However, these catalysts were suffered by mass transport because of their limited pore size and pore volume [15].

Concerned over this issue, it has focused attention on the mesoporous solid acid catalyst for biodiesel production because of their significant properties such as acidity and textural characteristics. Moreover, the mesoporous KIT-6 support has a three-dimensional cubic morphology with interpenetrating bicontinuous channels, which could be a superior catalytic support for solid acid catalyst synthesis [16, 17]. However, Heteropolytungstic acid (HPWA) is a strong Bronsted acid, which is significant in acid-catalyzed reactions and paid more attention to environmental protection and economic concern because of their non-toxic and inexpensive nature [18]. Furthermore, compared with mineral acids, HPWA showed higher catalytic activity for a wide verity of catalytic reactions [19–21]. However, in homogeneous systems, it highly suffered from the disadvantages like difficulty in separation of the catalyst from the reaction mixture and inconvenience for continuous production. These issues were overcome using HPWA-supported KIT-6 heterogeneous catalyst, synthesized by the hydrothermal and impregnation method. The impregnation of HPWA on KIT-6 support could significantly alter the textural properties of the catalyst. Furthermore, in the literature, various acid catalysts have been studied for neem oil transesterification, in which considerable activities were observed [22–28]. However, the use of these acid catalysts has been of less interest because of their toxicity, non-reusability, and restricted stabilities. Therefore, this problem has been recovered by heteropoly acid-supported KIT-6 catalyst, which has superior catalytic properties, i.e., resistance against pore blockage, high surface area, thicker pore walls, and interconnected 3D mesopores, which enhance the diffusion of the bulky molecule [29].

The present work reports for producing biodiesel via transesterification of neem oil using methanol as co-reactant. Further, a various weight percentage of $H_3PW_{12}O_{40}$ (10, 20, 30%) was impregnated on KIT-6 and it was characterized by different physicochemical techniques. Moreover, its catalytic activity was examined by liquid-phase transesterification of neem oil under different experimental conditions. Besides, various reaction parameters such as temperature, time, catalysts amount, and methanol, to oil ratios have been optimized. Finally, the recyclability of the optimized catalyst has been studied and its activity has been evaluated under optimized reaction condition. Therefore, this study could afford significant information on properties of HPWA/KIT-6 catalyst for improving the biodiesel yield via neem oil transesterification.

Experimental

Materials

Triblock copolymer (Pluronic P123, EO_{20} PO_{70} EO_{20}; Aldrich: Mol. Wt. 5800), tetraethylorthosilicate was obtained from Aldrich and Merck (98% pure). Hydrochloric acid, methanol, and *n*-butanol were obtained from SRL Biochem (India) Ltd, which was an AR-grade chemical. Commercial heteropoly acid such as $H_3PW_{12}O_{40}{\cdot}nH_2O$ was obtained from SRL Biochem (India) Ltd. Neem oil was purchased from the local market. All the chemicals were used as such without treatment.

Preparation of the catalysts

Mesoporous KIT-6 support was synthesized hydrothermally with molar ratios of 1 TEOS: 0.017 P123:1.83 HCl (35%):1.3 *n*-BuOH: 195 H_2O [30]. In a polypropylene bottle, pluronic P123 4 g, 144-g distilled water, and 7.9 g of 35% HCl were mixed and stirred for 4 h at 35 °C to an obtained homogeneous solution. And then, 4-g n-butanol as a co-solvent was added and stirring continued for another 1 h. After that, 8.6-g TEOS was added to the mixture and it was stirred for 24 h at 35 °C. Then, the whole mixture was placed in an air oven at 100 °C for 24 h. The obtained product was filtered and dried overnight in an air oven at 100 °C. The dried material was powdered and calcined at 540 °C for 8 h under the air atmosphere to remove the template.

Different (10, 20, 30%) weight percentage of HPWA were loaded on support by wet-impregnation method using dodecatungstophosphoric acid as the precursor. Pre-dried KIT-6 1 g and 20-mL deionized water were taken in a round bottom flask and stirred for few minutes. A desired amount of HPWA (e.g., 0.1 g for 10 wt%) was weighed and dissolved in 20-mL deionized water and this solution was added drop by drop to support material and stirred for 6 h. The residue was filtered and washed with deionized water. Finally, the impregnated material was dried at 100 °C and calcined in air

at 300 °C for 5 h [31]. The obtained material is represented as *X* % HPWA/KIT-6 (*X* = 10, 20, 30%).

Characterization techniques

XRD pattern of calcined support and catalyst was analyzed by XRD (Philips, Holland) using nickel-filtered Cu Kα radiation ($\lambda = 1.5406$ Å). The surface area of the catalyst was measured by the ASAP-2010 volumetric adsorption analyzer manufactured by the micrometrics corporation (Norcross, GA). Before measurement, each sample was degassed at 350 °C of pressure 10^{-5} Torr for 12 h in an outgassing station of the sorption apparatus. The nitrogen-sorption isotherms were obtained by BET method over different relative pressures; the pore size measurement and wall thickness were obtained by BJH method using nitrogen-sorption isotherms. The total acid content of all the HPWA-supported catalyst was measured by temperature-programmed desorption of ammonia (NH_3-TPD) in a flow reactor (micrometrics instrument corporation chemisoft TP × V1.02 unit 1-2750). The sample was pre-treated at 500 °C for 1 h in a flow of Helium, and then cooled to 100 °C with 10 vol.% NH_3 adsorption for half an hour. Further, the physisorbed ammonia was removed by purging with Helium until the baseline was stable at 100 °C, and then desorption started from 100 to 600 °C. The Bronsted and Lewis acid sites on the impregnated catalysts were analyzed by ex situ pyridine-adsorbed AT-FTIR technique using Perkin Elmer Spectrum Two spectrophotometer. About 100 mg of the samples were dried at 100 °C for 1 h. After drying, the sample was wetted with 0.3 mL of pyridine for 5 h. To remove the physisorbed pyridine from the wetted sample, it was heated at 120 °C for 1 h. After that the pyridine chemisorbed sample was mixed with KBr pellet, and the pellet was placed into the IR cell for recording the spectrum. The metal concentration in the impregnated catalyst was calculated by inductively coupled plasma optical emission spectrometry (ICP-OES) Perkin Elmer Optima 5300Dv instrument. Thermal gravimetric analysis (TGA) of support and catalysts was done on the waters TA instrument SDTQ 600. Surface morphology and elemental composition present in the catalyst were analyzed by HR-SEM with EDX using FEI Quanta FEG 200 instrument. The TEM images of support and HPWA-supported catalyst were analyzed by TECHNAI 10-Philphs instrument. The samples for TEM analysis were prepared by ultrasonic dispersion of catalyst in acetone for 1 h and dispersed samples were placed on a copper grid and samples were dried till the solvent was evaporated and further analyzed by TEM instrument. A diffuse reflectance UV–visible spectrum of the sample was recorded using JASCO V650 spectrophotometer and $BaSO_4$ was used as the reference.

Catalytic experiments

The activity of the catalyst was evaluated by the transesterification of neem oil using a liquid-phase reactor. In a typical transesterification reaction, 10 g of neem oil was added in 3 volumes of methanol with 0.35 g of the pre-treated catalyst. The reaction was carried out at 50–65 °C with reaction time 1–5 h; at the end of the reaction, the reaction mixture was cooled to room temperature and the catalyst was separated by filtration. The progress of the reaction was monitored by TLC. The crude reaction mixture was transferred to the water/n-hexane mixture of 1:3 ratios. The reaction mixture was separated into two layers using separating funnel. The lower layer consisted of water, glycerol, and methanol mixtures; whereas, the upper layer being the fatty acid alkyl esters, the un-reacted oil and intermediate products. After the removal of a solvent from the organic phase, the resulting composition was analyzed by the gas chromatograph (ShimazuGC-17A) equipped with an FID detector using (Rtx-5; 30 m × 0.25 mm id) column and the product was confirmed by ^{1}H NMR spectroscopy.

Results and discussion

X-ray diffraction study

The low-angle X-ray diffraction pattern of bulk HPWA, KIT-6, and HPWA-supported catalysts is represented in Fig. 1a. Low-angle XRD pattern showed diffraction peak at 0.89° (2θ) corresponding to (211) plane and a tiny peak at 1.1° (2θ) indexed to (220) plane, which was the characteristic of mesoporous KIT-6 materials. Furthermore, their unit cell parameter a_o value was calculated from the expression $a_o = \sqrt{6}d \times d_{(211)}$ and the values are represented in Table 1 [30, 31]. The intensity of the main reflection peak (211) gradually decreased with increasing HPWA loading in the catalyst and it was evidenced by the increasing of a_o value, and their values are shown in Table 1. Moreover, the diminishing of a peak in the catalyst could not affect the structure of KIT-6, as confirmed by retaining of mesopores in N_2 sorption isotherms, and it was shown in Fig. 2a, b. High-angle XRD patterns for bulk HPWA, KIT-6, and HPWA-loaded catalysts are represented in Fig. 1b. The highly sharp crystalline peak corresponding to bulk HPWA was observed in the 2θ range of 10–70 nm, which indicates a large crystalline phase of HPWA. However, on comparing with bulk HPWA, the peak intensity of HPWA-loaded catalysts was less; it may be due to the absence of bulk HPWA crystal phase on these catalysts, and it reveals that HPWA was highly dispersed on the KIT-6 support [32].

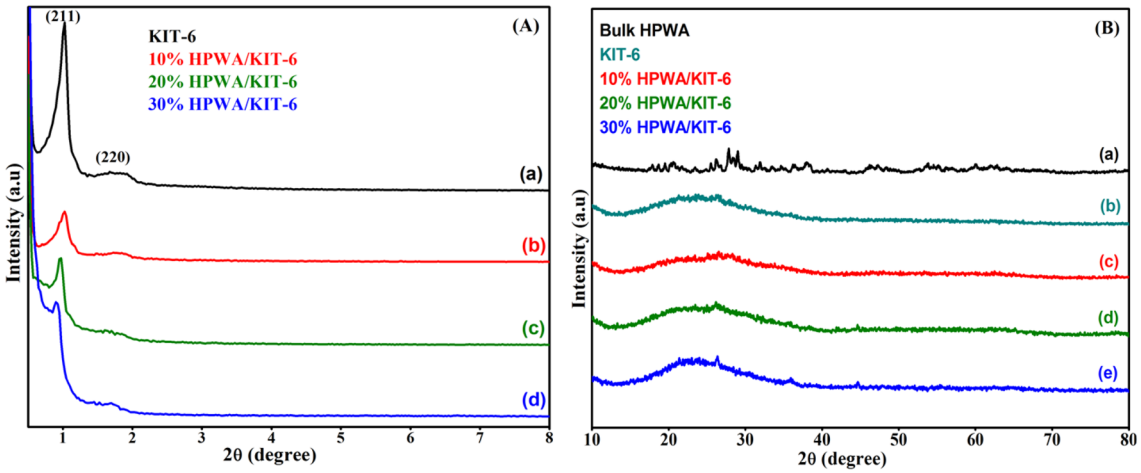

Fig. 1 XRD pattern of KIT-6 and heteropoly acid (HPWA)-supported KIT-6 catalysts. **a** Low-angle XRD pattern. **b** High-angle XRD pattern

Table 1 Textural properties, surface acidity, and metal content of support and supported catalysts

Catalysts	XRD despacing[a] (Å)	a_o (nm)	S^b_{BET} (m^2/g)	P^c_d (nm)	P^d_v (cc/g)	P^e_w(nm)	Acidity[f] (mmol/g)	ICP–OES W[g] (wt%)
KIT-6	87.7	21.4	704.6	9.3	1.3	1.4	–	–
10% HPWA/KIT-6	87.0	21.3	650.3	8.1	1.1	2.5	0.21	8.5
20% HPWA/KIT-6	92.2	22.5	635.7	8.1	0.6	3.1	0.28	15.3
30% HPWA/KIT-6	95.9	23.4	498.9	8.2	0.5	3.5	0.32	22.3

S_{BET} surface area, P_d pore diameter, P_w pore wall thickness

[a]Value obtained by low-angle XRD studies

[b]Surface area calculated by BET method using N_2-sorption isotherm

[c]Pore diameter (P_d) measured by BJH method from N_2-sorption analysis

[d]Pore volume estimated from N_2-sorption isotherm

[e]Pore Wall thickness of KIT-6 and HPWA-supported catalysts calculated by the definition [$P_w = a_{o/2} - P_D$ where, $a_o = \sqrt{6d \times d_{(211)}}$]

[f]Total acidity measured by NH_3-TPD analysis

[g]Values obtained by ICP–OES technique

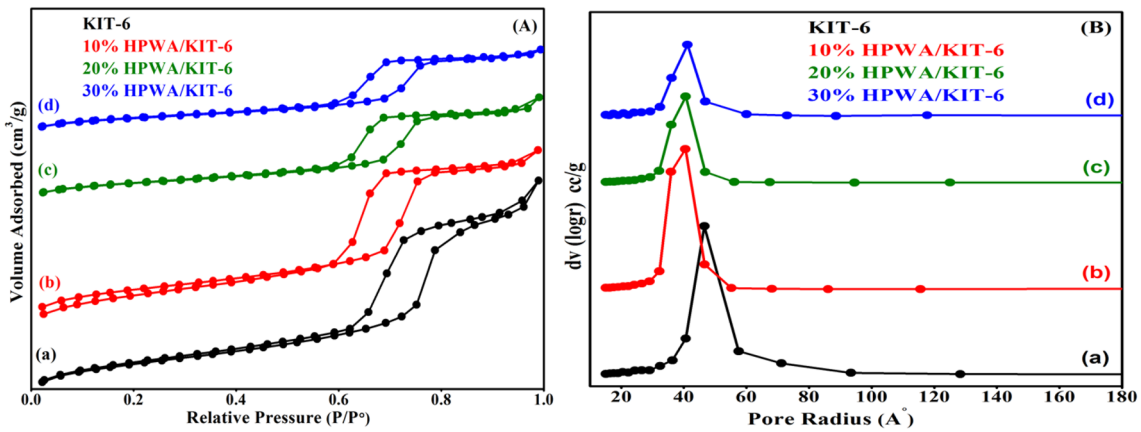

Fig. 2 **a** Nitrogen-sorption isotherm of KIT-6 and HPWA-supported catalysts. **b** BJH pore size distribution for KIT-6 and HPWA-supported catalysts

Nitrogen-sorption measurements

Nitrogen-sorption isotherms and their pore size distribution for the KIT-6 and HPWA-supported KIT-6 materials are shown in Fig. 2a, b, respectively. The BET surface area, average pore size and pore volume of all the prepared materials are shown in Table 1. The isotherms were assigned as type IV with capillary condensation of pore steps that occurred at 0.6–0.8, which was the characteristic of a large pore mesostructured material [33]. The surface area for KIT-6 support showed 704.6 m^2 g^{-1}. However, the surface area decreased in HPWA-supported catalysts on comparison with KIT-6 support, which may be due to the bulk HPWA species located on the external surface as well as on the pores of the catalyst [32]. The pore size distribution of KIT-6 and HPWA-loaded KIT-6 was calculated by the BJH method. The H1 broad hysteresis loop revealed that materials have good structural ordering with narrow pore size distribution [33]. However, the pore diameter was a maximum of 9.3 nm in KIT-6 support, whereas HPWA-supported catalyst shows 8.1 and 8.2 nm, respectively. The decreasing of pore diameter in HPWA-supported catalyst may be due to the partial pore block of support by bulk HPWA species.

Pyridine-adsorbed AT-FTIR spectroscopy study

Pyridine-adsorbed ATFT-IR spectra of KIT-6 support, bulk HPWA and HPWA-supported KIT-6 materials are presented in Fig. 3. The adsorption peak concerning KIT-6 was not observed, which confirmed the inertness of silica. However, the bulk HPWA showed a strong adsorption peak at 1445 cm^{-1} due to pyridine adsorbed on Lewis (L-Py) acid sites and the band appeared at 1493 cm^{-1} was characteristics of both Lewis (L-Py) and Bronsted (Py-H^+) acid sites [32, 34]. Besides, the HPWA supported catalyst shows band at 1493 cm^{-1} was due to pyridine adsorption on both Lewis (L-py) and Bronsted (L-H^+) acid sites and a band appeared at 1445 cm^{-1} was due to pyridine adsorbed on Lewis (L-Py) acid sites [32, 35]. Moreover, a small intense peak was appeared at 1545 cm^{-1} exhibiting Bronsted (Py-H^+) acid sites. These Bronsted acid sites formed on the catalyst due to the presence of small clusters of heteropoly acid [32, 35&36]. While, the Lewis acid sites were formed due to the interaction of heteropoly acid with framework silica [32]. The peak intensity of 10%, 20% and 30% HPWA-supported catalyst slightly increased with increasing HPWA loading of 10–30%. This indicates the increase of acidity with respect to HPWA loading; further, this result was supported by the quantified value obtained from NH_3-TPD analysis.

NH_3-TPD measurements

Figure 4 represented NH_3-TPD spectrum of 10% HPWA/KIT-6, 20% HPWA/KIT-6 and 30% HPWA/KIT-6 catalysts. The acidic strength of different weight percentages of heteropoly acid-supported KIT-6 catalyst was determined by the area under desorption of ammonia. Mostly, the acid sites were classified based on desorption temperature, in which the temperature in the range 25–200 °C corresponds to weak, and the ammonia desorption temperature 200–400 °C and above 400 °C indicate medium and strong acid sites, respectively [37, 38]. The NH_3-TPD spectrum of HPWA-supported catalysts showed desorption peak in the range of 100–390 °C indicating weak and medium acid sites. Their values are listed in Table 1, 0.21 mmol NH_3/g for 10% HPWA/KIT-6, 0.28 mmol NH_3/g for 20% HPWA/KIT-6 and 0.32 mmol NH_3/g for 30% HPWA/KIT-6. The highest amount of acidity

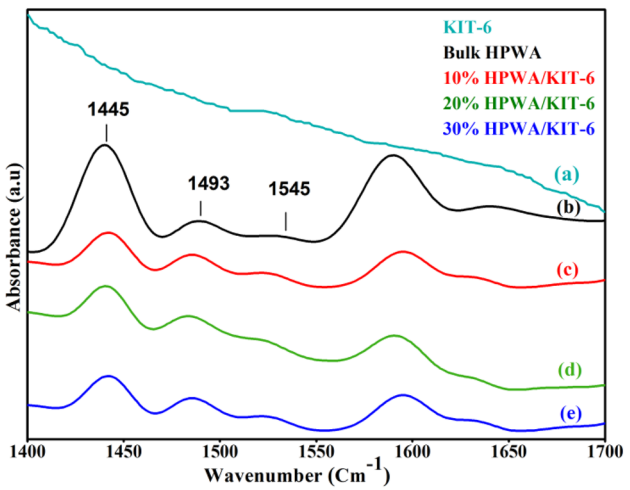

Fig. 3 Pyridine-adsorbed AT-FTIR spectra of KIT-6 and HPWA-supported catalysts

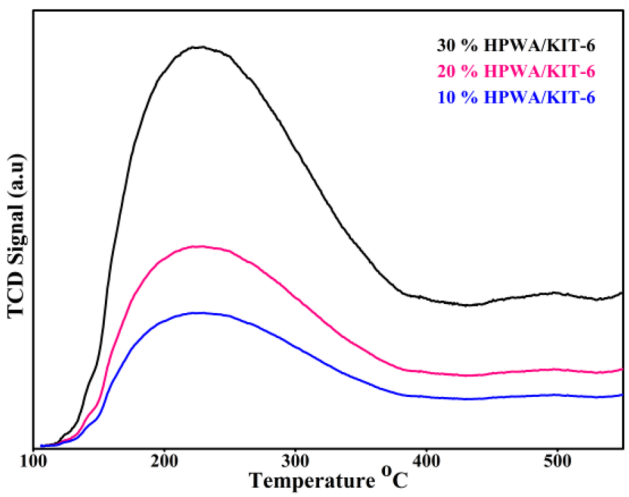

Fig. 4 Ammonia-TPD spectra of HPWA-supported KIT-6 catalysts

was observed in 30% HPWA catalyst, which may be due to the higher loading of heteropoly acid present on this catalyst.

Diffuse reflectance UV–visible spectroscopy (DRS-UV)

Figure 5 represents the DRS-UV visible spectra of bulk HPWA and 10%, 20%, 30% HPWA-supported KIT-6 catalysts. The metal ion coordination present in the framework or the extra framework in the catalyst was confirmed by this technique [39]. As represented in Fig. 5, the bulk HPWA sample shows a band at 260 nm, which confirms the presence of polyanions. However, HPWA-loaded catalyst shows broadband at 265 nm, and a small shift was characteristics of charge transfer in tungstophosphate anion $PW_{12}O_{40}^{3-}$ [40]. Also, this small shift was uniformly observed in all the supported catalyst, whereas the intensity sharply increased as the wt% increases. However, the bulk HPWA shows the additional broad signal at 360 nm, which was assigned as WO_3 clusters and these clusters were not seen in the HPWA-supported catalysts [40].

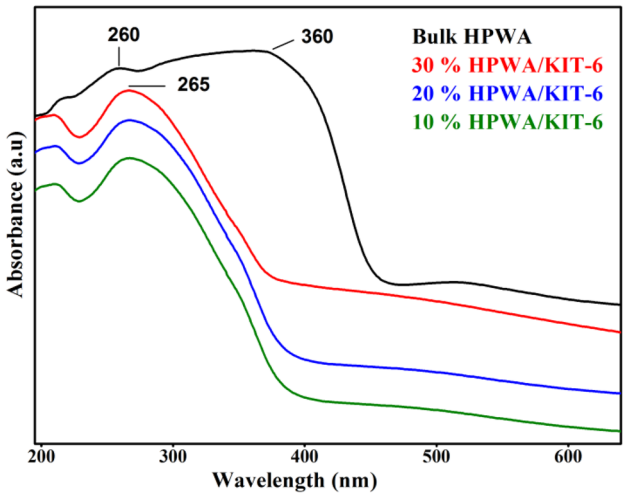

Fig. 5 UV–visible diffuse reflectance spectroscopy for bulk HPWA and HPWA supported catalysts

HR-SEM with EDAX analysis

Scanning electron microscopic images of KIT-6 and HPWA-supported KIT-6 catalysts are shown in Fig. 6. The morphology of the catalyst confirmed the typical images of mesoporous materials. However, the clear dispersion of heteropolyanion in the catalyst surface was not identified in this technique. Furthermore, the electron-dispersive X-ray spectrum (EDAX) of 20% HPWA/KIT-6 catalyst is represented in Fig. 6b which showed the presence of Si, O, P and W elements in this catalyst.

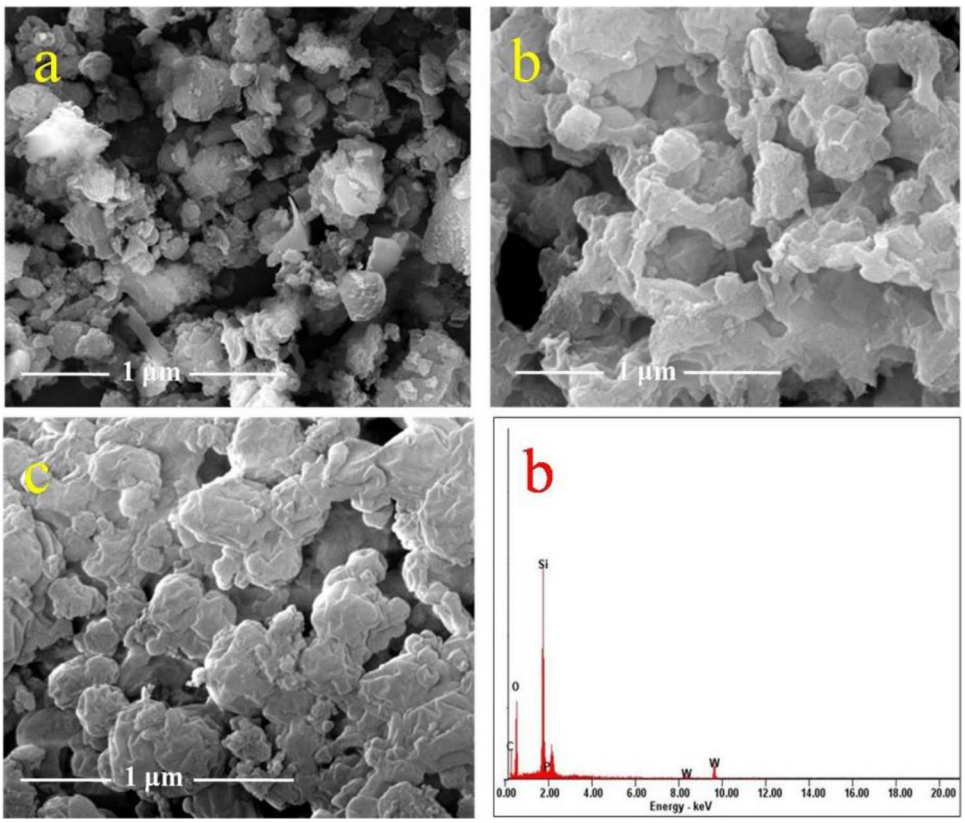

Fig. 6 HR-SEM images with EDAX spectrum of HPWA-supported catalysts. **a** 10% HPWA/KIT-6, **b** 20% HPWA/KIT-6 with EDAX spectrum, **c** 30% HPWA/KIT-6

Transmittance electron microscopy (TEM) study

TEM analysis investigates metal dispersion and surface morphology of support and HPWA-supported catalysts, which are shown in Fig. 7a–d. The TEM image of KIT-6 depicted in Fig. 7a revealed an open channel mesopore structure. However, the images represented in Fig. 7b–d for HPWA-supported catalysts were completely different from the original KIT-6 support. The distribution of smaller heteropoly acid particles on the catalyst surface was not seen, due to the formation of a heteropoly acid cluster on the catalyst surface. The dispersion of HPWA species on the catalyst surface was differed on a percentage of heteropoly acid loaded. Figure 7b illustrated a 10% HPWA-loaded catalyst, where the irregular distribution of heteropoly acid clusters was seen on the surface and further their pores were clearly observed. However, the clusters seen in the 20% HPWA-loaded catalyst were relatively smaller than the 10% HPWA-loaded catalyst. In the case of 30% HPWA-loaded catalyst, the heteropoly acid was highly diffused to surface and it shows higher pore blockage. The size of clusters was higher than the average pore size of HPWA-supported catalysts, which indicates that most of the particles were located on the external surface of the catalysts [36].

TGA analysis

The thermal stability of KIT-6 and HPWA-supported KIT-6 catalysts was investigated by TGA under the air atmosphere, which is represented in Fig. 8. The KIT-6 support shows degradation at 110 °C, due to water loss. However,

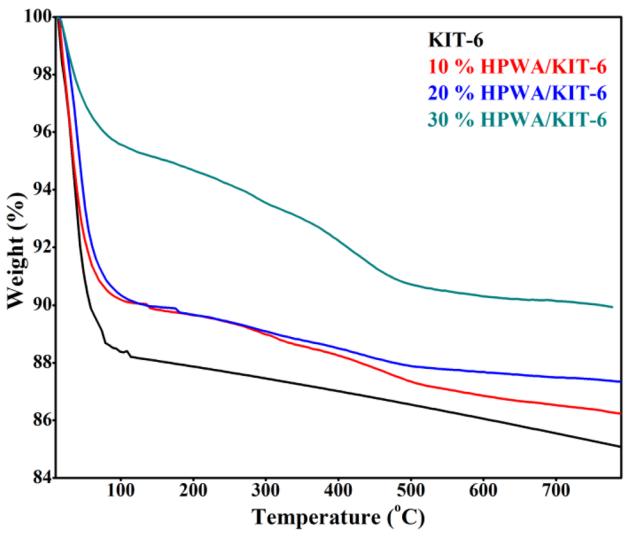

Fig. 8 Thermal gravimetric analysis of KIT-6, 10% HPWA/KIT-6, 20% HPWA/KIT-6 and 30% HPWA/KIT-6

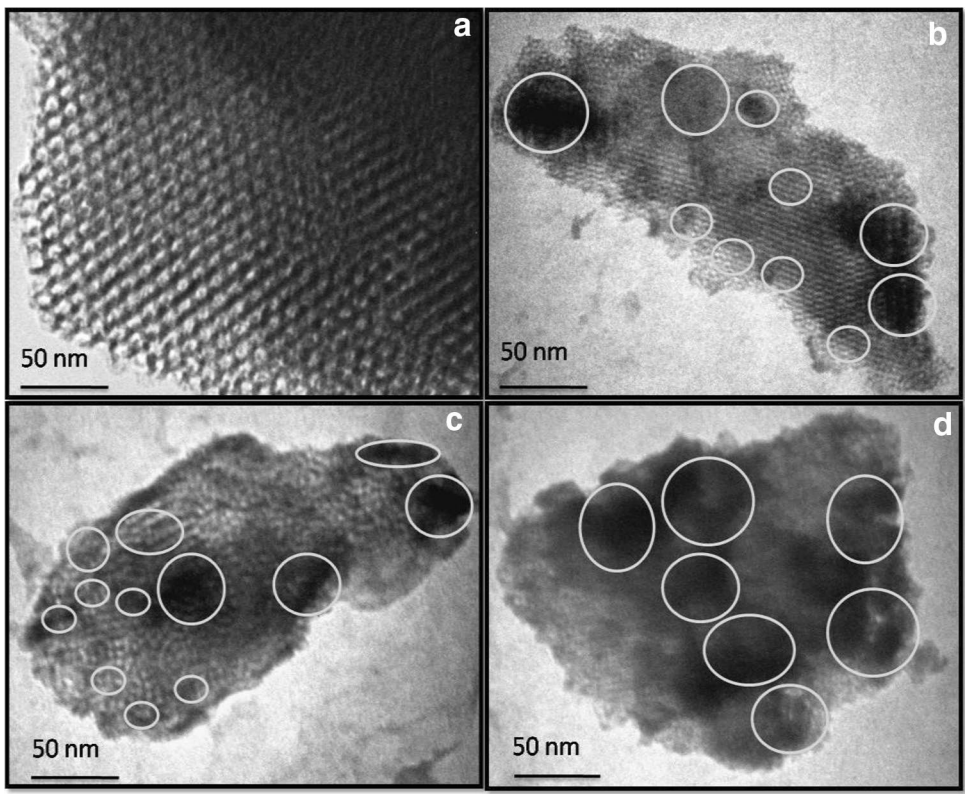

Fig. 7 TEM images of **a** KIT-6, **b** 10% HPWA/KIT-6, **c** 20% HPWA/KIT-6, and **d** 30% HPWA/KIT-6 catalysts

no degradation point was seen from 110 to 700 °C, which confirms that the KIT-6 withstand temperature up to 700 °C. Moreover, a different pattern was observed for HPWA-supported catalysts. All the supported catalyst showed degradation temperature below 110 °C due to physisorbed water. Nevertheless, a small degradation was observed at 200 °C due to the loss of water molecules per Keggin unit of heteropoly acid [41]. However, the degradation observed at 460 °C was due to the loss of acidic protons and the starting decomposition point of Keggin structure [42].

Catalytic studies

Effect of heteropoly acid loading over KIT-6

The transesterification activity of different wt% loaded HPWA catalysts is represented in Fig. 9. The loading of HPWA has a significant impact on the conversion of neem oil, particularly, 20% HPWA/KIT-6 catalyst showed higher conversion. The increasing order of trans-esterification activity was 20% HPWA/KIT-6 (90%) > 30% HPWA/KIT-6 (82%) > 10% HPWA/KIT-6 (70%), respectively. Among the catalyst, 10% of HPWA shows that lower conversion may be due to the low loading of HPWA. Furthermore, 30% HPWA catalyst shows conversion lesser than that of 20% HPWA catalyst, due to their high HPWA amount, it reduces surface area and pore volume. However, the higher conversion was obtained for 20% HPWA/KIT-6 due to their medium acid sites and moderate acid values, and these values lie in-between the 10% and 30% HPWA catalyst. Not only that, their surface area (635.7 m^2/g), pore volume (0.6 cc/g), optimum tungsten percentage from ICPOES 15.3% and fine dispersion of small clusters of HPWA on the catalyst surface play a significant role in higher neem oil conversion.

Effect of reaction temperature

The effect of reaction temperature on the conversion of neem oil with methanol over 20% HPWA/KIT-6 catalyst was investigated in the temperature between 50 and 65 °C at 3 h under liquid-phase condition, which is represented in Fig. 10. The conversion increases on increasing reaction temperature and the maximum conversion 88% achieved at 60 °C. Initially, monoglycerides (MG) and diglycerides (DG) were obtained at lower temperatures and on increasing the temperatures, these glycerides were fully converted into FAME (Fatty acid methyl ester) even though a trace quantity of monoglyceride was obtained. From this study, the reaction temperature of 60 °C was identified as the optimum for further reaction.

Effect of reaction time

Figure 11 illustrated the conversion and selectivity of neem oil with respect to run duration. Neem oil conversion of 90% was achieved at 3 h with 20% HPWA/KIT-6 catalyst. The influence of reaction time was significant in 20% HPWA/KIT-6 catalyst. It shows that the conversion increased 1–3 h, and after 3 h, the conversion decreased. It may be due to the deactivation of the catalyst under these reaction conditions. However, the FAME selectivity was obtained at all run duration and the maximum FAME was observed at beyond 3 h. Initially, the conversion of MG and DG was low and on

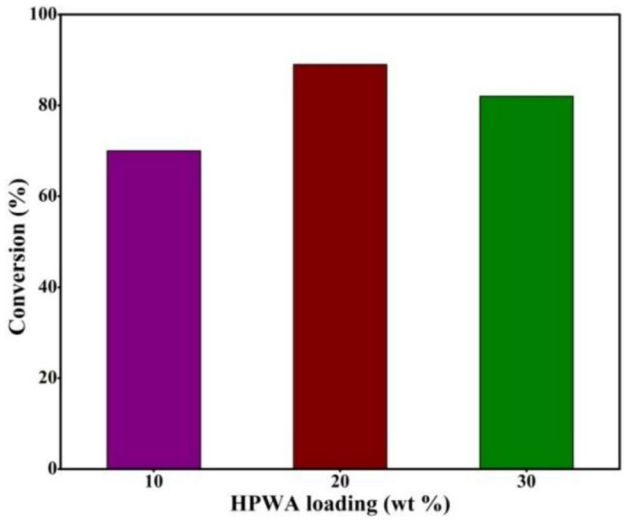

Fig. 9 Influence of HPWA loading over KIT-6 in the transesterification of neem oil [Reaction condition: catalyst, 0.35 g; oil, 10 g; 60 °C; run time, 3 h; MeOH/oil (mole), 10]

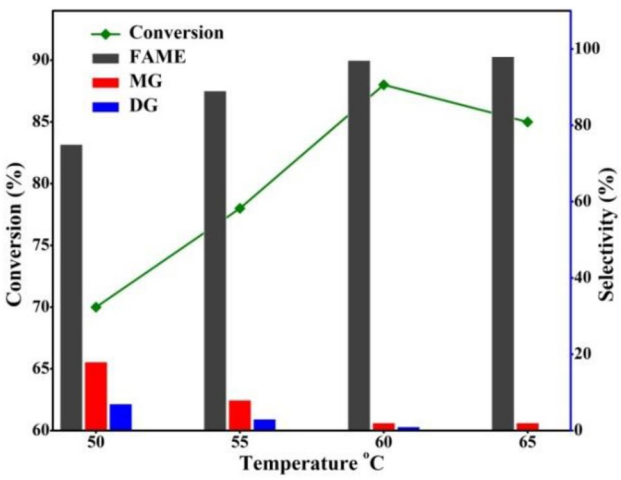

Fig. 10 Effect of reaction temperature over 20% HPWA/KIT-6 in transesterification of neem oil [Reaction condition: catalyst, 0.35 g; oil, 10 g; 50–65 °C; run time, 3 h; MeOH/oil (mole), 10]

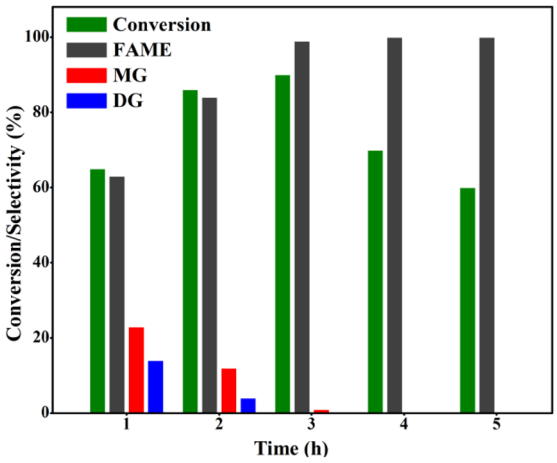

Fig. 11 Effect of reaction time with respect to 20% HPWA/KIT-6 in transesterification of neem oil [Reaction conditions: catalyst, 0.35 g; oil, 10 g; 60 °C; run time, 1–5 h; MeOH/oil (mole), 10]

increasing the time, their conversion increased, which may be due to the rapid FAME desorption [43].

Effect of MeOH/oil molar ratio

The effect of oil to methanol molar ratio for neem oil conversion and FAME selectivity is represented in Fig. 12. The influence of oil to methanol molar ratio creates a significant improvement in the transesterification of neem oil. However, the conversion increases on increasing the oil to methanol ratio and the maximum conversion 100% was obtained in higher methanol ratio; it reveals that the maximum methanol content in the reaction mixture could increase the

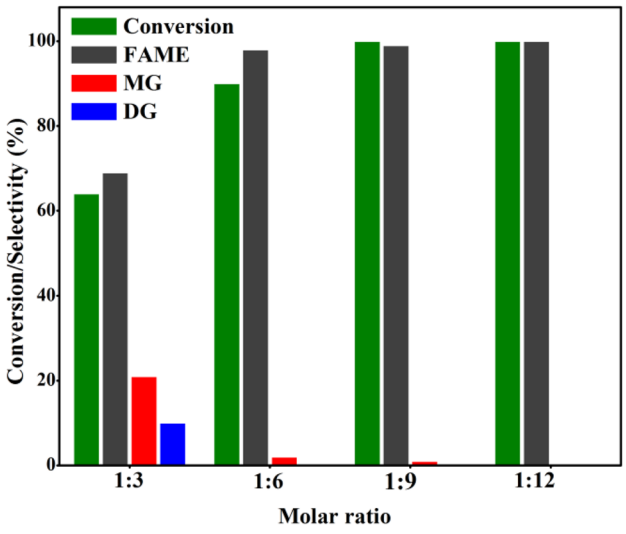

Fig. 12 Effect of MeOH/oil ratio with respect to 20% HPWA/KIT-6 in transesterification of neem oil (reaction conditions: catalyst, 0.35 g; oil, 10 g; 60 °C; run time, 3 h)

triglyceride conversion [44], and also the product selectivity of FAME significantly increased at higher methanol ratio.

Reusability

The reusability and reproducibility of a 20% HPWA/KIT-6 catalyst were studied under optimum reaction conditions. Once the reaction was completed, the catalyst was recovered by filtration and followed by acetone wash. Further, the catalyst was dried and reused for a consequent experiment, after the addition of new oil and methanol under the optimum conditions. In the first catalytic cycle, it showed conversion of 84% and after succeeding cycles, the conversion decreased which may be due to loss of tungsten in the reaction mixture. These results suggested that 20% HPWA/KIT-6 catalyst significantly showed conversion of 80% up to three cycles. The leaching of tungsten species in 20% HPWA/KIT-6 catalyst was measured by ICP–OES techniques, which is represented in Table 2. The tungsten wt% obtained from these techniques towards the succeeding reaction cycles, i.e., first, second and third for 20% HPWA/KIT-6 catalyst was 12.3, 11.2 and 10.8, respectively. Furthermore, the tungsten loss was observed maximum in the first cycle; whereas in the second and third cycles, it decreased.

Conclusions

Three different weight percentages of heteropoly acid-supported mesoporous KIT-6 catalysts were synthesized by wet-impregnation method, characterized and applied to liquid-phase neem oil transesterification to fatty acid methyl ester. The order of trans-esterification activity was 20% HPWA/KIT-6 (90%) > 30% HPWA/KIT-6 (82%) > 10% HPWA/KIT-6 (70%), respectively. About 90% conversion and high FAME yield were observed in 20% HPWA catalyst. Furthermore, the catalyst possesses the nature of Bronsted acid sites, large surface area, pore size, and fine dispersion

Table 2 Recyclability of 20% HPWA/KIT-6 catalyst

Cycles	W^a (wt%)	Conversion (%)	W^b (wt%)	Yield of FAME (%)
Fresh	15.3	90	–	98
1	12.3	84	2.8	93
2	11.2	80	1.0	90
3	10.8	78	0.2	85

Reaction condition: catalyst, 0.35 g; oil, 10 g; 60 °C; run time, 3 h; MeOH/oil (mole), 10

[a]Tungsten content in 20% HPWA/KIT-6 taken by ICP–OES technique

[b]Tungsten present in reaction mixture after every cycles measured by ICP–OES technique

of small HPWA clusters on the surface was responsible for higher neem oil conversion, further these results well agreed with N_2-Sorption and TEM analysis. Besides, the higher loading of 30% HPWA catalyst could not give higher conversion when compared with 20% HPWA catalyst, because their low surface area and bulk species of HPWA highly block the pore size of the catalyst. The leaching study of the 20% HPWA catalyst, combined with the analysis of leached tungsten, indicated that the tungsten species practically leached as maximum as 4% up to three cycles in the reaction mixture under hydrothermal reaction condition.

Acknowledgements The author acknowledges UGC-BSR, New Delhi, India for providing financial support to carry out this research. Also, he thank the Department of Chemistry, IIT Madras, Chennai for providing instrumentation facility.

References

1. Wang, Y., Wang, D., Tan, M., Jiang, B., Zheng, J., Tsubaki, N., Wu, M.: Monodispersed hollow SO_3H—functionalized carbon/silica as efficient solid acid catalyst for esterification of oleic acid. ACS Appl. Mater. Interfaces. **7**(48), 26767–26775 (2015)
2. Boey, P.L., Ganesan, S., Maniam, G.P., Khairuddean, M., Lee, S.E.: A new heterogeneous acid catalyst system for esterification of free fatty acids into methyl esters. Appl. Catal. A **12–7**, 433–434 (2012)
3. Kiss, A.A., Dimian, A.C., Rothenberg, G.: Solid acid catalysts for biodiesel production—towards sustainable energy. Adv. Synth. Catal. **75–81**, 348 (2006)
4. Semwal, S., Ajay, K., Rajendra, A.P., Deepak, B.K., Tuli, : Biodiesel production using heterogeneous catalysts. Bioresour. Technol. **102**, 2151–2161 (2011)
5. Liu, W., Yin, P., Liu, X., Chen, W., Chen, H., Liu, C.: Microwave assisted esterification of free fatty acid over a heterogeneous catalyst for biodiesel production. Energy Convers Manag **76**, 1009–1014 (2013)
6. Berchmans, H.J., Hirata, S.: Biodiesel production from crude *Jatropha curcas* L. seed oil with a high content of free fatty acids. Bioresour. Technol. **99**, 1716–1721 (2008)
7. Anindita, K., Subrata, K., Souti, M.: Biodiesel production from neem towards feedstock diversification: Indian perspective. Renew. Sustain. Energy Rev. **16**, 1050–1060 (2012)
8. Muthu, H., SathyaSelvabala, V., Varathachary, T.K., Selvaraj, D.K., Nandagopal, J., Subramanian, S.: Synthesis of biodiesel from neem oil using sulphated zirconia via tranesterification. Braz. J. Chem. Eng. **27**, 601–608 (2010)
9. Hasan Ali, M.D., Mashud, M., Rowsonozzaman Rubel, M.D., Ahmad, R.H.: Biodiesel from Neem oil as an alternative fuel for diesel engine. Proc. Eng. **56**, 625–630 (2013)
10. Kareem, M.O., Guerrero Pena, D.J., Raj, A., Alrefaai, M.M., Stephen, S., Anjana, T.: Effects of neem oil derived biodiesel addition to diesel on the reactivity and characteristics of combustion-generated soot. Energy Fuels **31**, 10822–10832 (2017)
11. Atabani, A.E., Silitonga, A.S., Ong, H.C., Mahlia, T.M.I., Masjuki, H.H., Badruddin, I.A.: Non-edible vegetable oils: a critical evaluation of oil extraction, fatty acid compositions, biodiesel production, characteristics, engine performance and missions production. Renew. Sustain. Energy Rev **18**, 211–245 (2013)
12. Abebe, K., Endalew, A., Kiros, Y., Zanzi, R.: Inorganic heterogeneous catalysts for biodiesel production from vegetable oils. Bio Mass Bioenergy **35**, 3787–3809 (2011)
13. Kiss, A.A., Dimian, A.C., Rothenberg, G.: Biodiesel by catalytic reactive distillation owered by metal oxides. Energy Fuels **22**, 598–604 (2008)
14. Shao, G.N., Sheikh, R., Hilonga, A., Lee, J.E., Park, Y.H., Kim, H.T.: Biodiesel production by sulfated mesoporous titania-silica catalysts synthesized by the sol-gel process from less expensive precursors. Chem. Eng. J. **215–216**, 600–607 (2013)
15. Kloetstra, K.R., Bekkum, V.H.: Base and acid catalysis by the alkali-containing MCM-41 mesoporous molecular sieve. J. Am. Chem. Soc. **1**, 1005–1006 (1995)
16. Tüysüz, H., Lehmann, C.W., Bongard, H., Tesche, B., Schmidt, R., Schüth, F.: Direct imaging of surface topology and pore system of ordered mesoporous silica (MCM-41, SBA-15, and KIT-6) and nanocast metal oxides by high resolution scanning electron microscopy. J. Am. Chem. Soc. **130**(115), 10–17 (2008)
17. Chermahini, N.A., Andisheh, N., Teimouri, A.: KIT-6-anchored sulfonic acid groups as a heterogeneous solid acid catalyst for the synthesis of aryl tetrazoles. J. Iran. Chem. Soc. (2018). https://doi.org/10.1007/s13738-017-1282-y
18. Alsalme, A., Elena, F., Ivan, K.V., Kozhevnikov, A.: Heteropoly acids as catalysts for liquid-phase esterification and transesterification. Appl. Catal. A Gen. **349**, 170–176 (2008)
19. Kozhevnikov, I.V., Kloetstra, K.R., Sinnema, A., Zandbergen, H.W., Van Bekkum, H.: Study of catalysts comprising heteropoly acid $H_3PW_{12}O_{40}$ supported on MCM-41 molecular sieve and amorphous silica. J. Mol. Catal. A: Chem. **114**, 287–298 (1996)
20. Brahmkhatri, V., Patel, A.: Esterification of lauric acid with butanol-1 over H3PW12O40 supported on MCM-41. Fuel **102**, 72–77 (2012)
21. Dharshini, D., Bala, A., Souza, K.D., Misra, M., Chidambaram, D.: Conversion of a variety of high free fatty acid containing feedstock to biodiesel using solid acid supported catalyst. J. Clean. Prod. **104**, 273–281 (2015)
22. Alia, H.M.D., Mashud, M.M.D., Rubel, R., Ahmad, R.H.: Biodiesel from Neem oil as an alternative fuel for Diesel engine. Proc. Eng. **56**, 625–630 (2013)
23. Adam, F., James, L.A., Bennett, A., Jinesh, C., Manayil, A., Wilson, K.: Heterogeneous catalysis for sustainable biodiesel production via esterification and transesterification. Chem. Soc. Rev. **43**, 7887 (2014)
24. Karmakar, A., Biswas, P.A., Mukherjee, S.: Environment-congenial biodiesel production from non-edible neem oil. Environ. Eng. Res. **17**(S1), S27–S32 (2012)
25. Shruthi, H., Heroor, A., Rahul Bharadwaj, S.D.: Production of bio-fuel from crude neem oil and its performance. Int. J. Environ. Eng. Manag. **4**, 425–432 (2013)
26. Sathya, T., Manivannan, A.: Biodiesel production from neem oil using two step transesterification. Int. J. Eng. Res. Appl. **3**, 488–492 (2013)
27. Muthu, H., SathyaSelvabala, V., Varathachary, T.K., Kirupha Selvaraj, D., Nandagopal, J., Subramanian, S.: Synthesis of biodiesel from neem oil using sulphated zirconia via tranesterification. Braz. J. Chem. Eng. **27**, 601–608 (2010)
28. Jibril, M., Joel, A.S., Edith, U., Audu, A.A.: Production and characterization of biodiesel from jatropha oil and neem oil. Int. J. Emerg. Trends Eng. Dev. **2**, 2 (2012)

29. Jermy, B.R., Cho, D.R., Bineesh, K.V., Kim, S.Y., Park, D.W.: Direct synthesis of vanadium incorporated three-dimensional KIT-6: a systematic study in the oxidation of cyclohexane. Microporous Mesoporous Mater. **115**, 281–292 (2008)
30. Karthikeyan, G., Pandurangan, A.: Post synthesis alumination of KIT-6 materials with Ia3d symmetry and their catalytic efficiency towards multicomponent synthesis of 1H-pyrazolo[1,2-]phthalazine-5,10-dione carbonitriles and carboxylates. J. Mol. Catal. A: Chem. **361–362**, 58–67 (2012)
31. Sudhakar, P., Pandurangan, A.: Rh/Ni wet-impregnated Ia3d mesostructured aluminosilicate and r-GO catalysts for hydrodeoxygenation of phenoxybenzene. New J. Chem. **41**, 7893–7907 (2017)
32. Karthikeyan, G., Pandurangan, A.: Heteropolyacid ($H_3PW_{12}O_{40}$) supported MCM-41: an efficient solid acid catalyst for the green synthesis of xanthenedione derivatives. J. Mol. Catal. A: Chem. **311**, 36–45 (2009)
33. Ramanathan, A., Subramaniam, B., Maheswari, R., Hanefeld, U.: Synthesis and characterization of Zirconium incorporated ultra large pore mesoporous silicate, Zr–KIT-6. Microporous Mesoporous Mater. **167**, 207–212 (2013)
34. Bhagiyalakshmi, M., Herbert Mabel, J., Vishnupriya, S., Palanichamy, M., Murugesan, V.: Selective epoxidation of dimethyl maleate to *cis*-epoxydimethyl succinate over solid acid catalysts. Catal. Today **141**, 234–241 (2009)
35. Satish Kumar, G., Vishnuvarthan, M., Palanichamy, M., Murugesan, V.: SBA-15 supported HPW: effective catalytic performance in the alkylation of phenol. J. Mol. Catal. A: Chem. **260**, 49–55 (2006)
36. Ajaikumar, S., Pandurangan, A.: HPW and supported HPW catalyzed condensation of aromatic aldehydes with aniline: synthesis of DATPM derivatives. J. Mol. Catal. A: Chem. **286**, 21–30 (2008)
37. Chen, Y., Cao, Y., Suo, Y., Zheng, G.P., Guan, X.X., Zheng, Z.C.: Mesoporous solid acid catalysts of 12-tungstosilicic acid anchored to SBA-15: characterization and catalytic properties for esterification of oleic acid with methanol. J. Taiwan Inst. Chem. Eng. **51**, 186–192 (2015)
38. Kalpesh, D., Jitendra P.R., Radha S.V., Jayaram.: Silica supported heteropolyacid catalyzed dehydration of aldoximes to nitriles and alcohols to alkenes. Green Chem. Lett. Rev. **4**(2), 143–149 (2011)
39. Nandhini, U., Banumathi Arabindoo, K., Palanichamy, M., Murugesan, V.: Al-MCM-41 supported phosphotungstic acid: application to symmetrical and un symmetrical ring opening of succinic anhydride. J. Mol. Catal. A Chem. **243**, 183–193
40. Sheng, X., Zhou, Y., Zhang, Y., Xue, M., Duan, Y.: Immobilization of 12tungstophosphoric acid on LaSBA-15 and its catalytic activity for alkylation of *o*-xylene with styrene. Chem. Eng. J. **179**, 295–301 (2012)
41. Jose, A., Dias, Rangel, M.D.C., Silvia, C.L., Dias, Caliman, E., Fillipe A.C., Garcia.: Benzene transalkylation with C9 + aromatics over supported 12-tungstophosphoric acid on silica catalysts. Appl. Catal. A Gen. **328**, 189–194 (2007)
42. Obal, Z., Dogu, T.: Activated carbon–tungstophosphoric acid catalysts for the synthesis of tert-amyl ethyl ether (TAEE). Chem. Eng. J. **138**, 548–555 (2008)
43. Sankaranarayanan, T.M., Pandurangan, A., Banu, M., Sivasankar, S.: Transesterification of sunflower oil over MoO_3 supported on alumina. Appl. Catal. A **410**, 239–247 (2011)
44. Udayakumar, V., Pandurangan, A.: Catalytic activity of mesoporous V/SBA-15 in the transesterification and esterification of fatty acids. J. Porous Mater. **21**, 921–931 (2014)